SPH modeling of fast muddy debris flow: numerical and experimental comparison of certain commonly utilized approaches

Ital. J. Geosci. (Boll. Soc. Geol. It.), Vol. 132, No. 3 (2013), pp. 350-365, 11 figs., 3 tabs. (doi: 10.3301/IJG.2013.01)

SPH modeling of fast muddy debris flow: numerical and experimental comparison of certain commonly utilized approaches

Antonio Pasculli (*), Lorenzo Minatti (**), Nicola Sciarra (*) & Enio Paris (**)

ABSTRACT

SPH (Smoothed Particle Hydrodynamics) is a particle, purely mesh-free Lagrangian method, proposed by different authors, well suited to the computing of highly transitory free surface flows of complex fluids in complex geometries. Different approaches have been proposed in order to better simulate the mutual interaction between particles and their interactions with boundaries.

Therefore, the main target of this article is to discuss and explore the numerical performance of certain commonly utilized SPH approaches, based essentially on mass and momentum balances, in the simulation of a 2D fast mudflow in fast motion, composed of fluid and solid material, assumed to be just one equivalent phase (fluid-solid). The "Herschel-Bulkley", non Newtonian constitutive equations, describing a viscoplastic material suitable to reproduce the rheological behaviour of mudflows, has been selected. Hence, a laboratory experimental test, already proposed in literature and, after properly scaling, representative of a real fast flow phenomenon, was considered for comparison with numerical outcomes carried out by a research code that has already been tested and discussed in previous papers. A simple but effective statistical approach was developed and applied in order to identify and utilize a numerical index suitable for the quantitative measurement of the degree of matching between numerical results and measurement data affected by experimental errors. More than thirty numerical experiments were performed, of which the most significant eleven simulations are discussed. Satisfactory results were achieved. As outcomes, it was verified that, in particular for the selected experimental test, Rusanov flux addition within the continuity equation with the proper choice of both the viscosity term of momentum and the SPH boundary conditions, is suited to enhancing the performance of this type of numerical simulation of a fast flow.

Key words: *SPH, 2D numerical modeling, parametric studies, landslide in fast motion, muddy debris flow.*

INTRODUCTION

In recent years, the hazard of catastrophic landslides due to the increase of hydro-geological risk has assumed the importance of a remarkable emergency, provoking many casualties and material damage. In the specific, following intense torrential rainfall, if slopes are covered by water saturated soils or fine grained sedimentary deposits, such material may become liquefied resulting in a fast movement of large quantities of material. There are many proposed classifications of this kind of phenomena: Varnes (1954), Coussot & Meunier (1996), Cruden & Varnes (1996), Hungr *et alii* (2001), Takahashi (2001). Among the identified phenomena, earthflow, debris flow, muddy-debris-flow and muddy-flow are proposed classification relating to rapid gravity-driven unsteady flows of highly concentrated mixtures of water and solid material with large grain size distribution and with complex internal structures. The type of fast landslide flow discussed by the study that this article refers to, is assumed to be similar to a muddy debris flow, characterized by a mixture of water and poorly sorted granular material flowing under the effect of gravity (Coussot & Meunier, 1996; Laigle & Coussot, 1997; Iverson, 1997; Crosta *et alii*, 2001; Iverson *et alii*, 2010).

The most widely used approaches to model muddy debris flow or debris flows in general are usually related either to "continuum" or to "granular" mechanics. The content of this paper belongs to the former type of approach where the Navier-Stokes equations are considered as the master tool. Having stated this, in the "continuum" framework, a fairly general mathematical model that can be used to model a physical phenomenon similar to the one discussed in this paper would consist of two sets of equations: the first for the liquid phase and the second for the solid phase. Interaction terms can then be added to the equations in order to model the forces exchanged by the two phases. A model of this kind can be derived from the mixture theory (Atkin & Craine, 1976): an implementation of such approach in the case of debris flows can be found in Iverson (1997), where the possibility of using different rheological models for each phase is suggested. Grain size distribution plays an important role in the physics of this type of phenomenon and developments in the study of water-solid mixtures have shown that the clay fraction can also be of great importance, as it influences the granular interactions. In particular, it is reported by Laigle & Coussot (1997) that muddy debris flow mixtures with a high clay fraction, despite retaining their two-phase nature, behave as viscoplastic fluids and that a single phase model of such kind can reproduce their physics to a good degree of approximation. We thus restrict our analysis to the specific case of debris flows characterized by a high clay fraction (mudflows) and simplify the problem by employing a single equivalent phase model of a viscoplastic fluid. Moreover, as simplifying approximation, concentration fluctuations, segregation, sedimentation and transition from laminar to turbulence regime were neglected. Additionally the complex phenomena occurring at the front of the flow were not included.

(*) Department of Engineering and Geology (INGEO), University G. d'Annunzio Chieti-Pescara, Italy. Corresponding author: Department of Engineering and Geology (INGEO), University of Chieti-Pescara (Italy); Via dei Vestini, 31 - 66013 Chieti; University G. d'Annunzio Chieti-Pescara (Italy); Office phone number: 39 0871 355 6159; fax: 39 0871 355 5364; a.pasculli@unich.it

(**) Department of Civil and Environmental Engineering, University of Florence, Italy. Via S. Marta, 3 - 50139 Firenze (Italy).

The bibliography relating to numerical approaches is very extensive and, for the sake of completeness, we mention the fields of Computational Fluid Dynamics (CFD), and of Computational Granular Dynamics (CGD). CFD (CHUNG, 2006; among many others) and CGD (PÖSCHEL & SCHWAGER, 2005) are considered, respectively, as numerical tools relating to continuum mechanics and Molecular Dynamics, used to simulate landslide flow. Nevertheless, according to the scope of the present paper, a CFD numerical method was selected from those suitable for solving the Navier-Stokes equations. Finite Elements (FEM), Finite Volumes (FVM), Finite Differences (FDM) and Depth-Averaged Approach (Shallow Water Model) are some of the most commonly used methods (CHUNG, 2006). For all the afore-mentioned approaches, grid generation is an important step to be performed. Other important issues relating to the numerical solutions of fluid flow problems modelled with the Navier-Stokes equations involve incompressibility and non linearity of convective terms. In order to avoid the latter, a Lagrangian approach is commonly selected instead of an Eulerian one. Furthermore, particular care should be taken concerning the numerical issues relating to large deformations. This is the main reason why a frequent (CPU time consuming) update of the grid, aimed at lowering the excessive mesh distortion due to large deformations, is often necessary. From the above discussion, it is clear that methods that avoid the numerical instability due to convective terms, lower grid generation time and that are capable of easily taking free surfaces and violent mass fluxes into account, are highly desirable. "Meshless Finite Element Methods" include many of the above necessary discussed features (see IDELSOHN *et alii*, 2003 for an overview). The "Smoothed Particle Hydrodynamics" (SPH), briefly described in the following paragraphs and selected in our approach, is one such method (LIU & LIU, 2010; CHAMBON *et alii,* 2011). There are many proposed SPH approaches which differ from one another due to important numerical calculation features, regarding essentially pressure, mass flow, inter-particle viscosity and boundary conditions. Thus, in order to provide a 2D flexible tool, suited to the easy implementation and testing of different numerical approaches proposed in literature, we developed and implemented a research computer code (MINATTI & PASCULLI, 2010, 2011), written in 1995 Fortran language. Due to the lack of accurate field data experimental results obtained from laboratory tests (LAIGLE & COUSSOT, 1997) were selected. Such experimental data was used for comparisons with numerical results obtained with the different SPH approaches implemented in our code. The comparisons essentially regarded the arrival times of the debris front flow at specific locations in a laboratory flume. Several CPU time consuming numerical simulations (more than thirty) were carried out, but only the most significant eleven simulations will be discussed in the following paragraphs.

MATHEMATICAL MODELING

In light of the considerations reported in the introduction, we are therefore interested in the equations of motion of an incompressible viscous non-Newtonian fluid. In order to develop a theoretical framework for a numerical model we resorted to the basic balance equations governing the motion of a continuum, namely mass conservation and momentum equations. They can be written in Lagrangian form as:

$$\frac{D\rho}{Dt} + \rho \nabla \cdot \underline{\mathbf{v}} = 0 \tag{1}$$

$$\rho \frac{D\underline{\mathbf{v}}}{Dt} = \rho \underline{\mathbf{f}} + \nabla \cdot \underline{\underline{\boldsymbol{\sigma}}} \tag{2}$$

Where: $\underline{\mathbf{v}}$ is the local velocity of the continuum; ρ is the local density of the continuum; $\underline{\mathbf{f}}$ is the body force per unit of mass exerted on the continuum; $\nabla \cdot$ is the 'divergence' symbol; $\underline{\underline{\boldsymbol{\sigma}}}$ is the total local stress tensor. The total stress tensor is usually split into two parts: an isotropic and a deviatory one: The stress tensor decomposition is indicated as follows in the paper: $\underline{\underline{\boldsymbol{\sigma}}} = -p\underline{\underline{\mathbf{I}}} + \underline{\underline{\boldsymbol{\tau}}}$, where: p is the isotropic pressure; $\underline{\underline{\mathbf{I}}}$ is the unit tensor; $\underline{\underline{\boldsymbol{\tau}}}$ is the deviatory part of the total stress tensor. The constitutive equation of the deviatory part of the total stress tensor, for a viscous compressible fluid, can be written as the sum of two terms: the first one depending on the shear viscosity and the other one on the bulk viscosity. The latter acts only when volume variations occur ($\nabla \cdot \underline{\mathbf{v}} \neq 0$), as in the case of compressible fluid. However, as common practice, an incompressible fluid can also be studied as a weak compressible one, thus bulk viscosity may affect numerical results. A wide class of fluid rheologies can be described in terms of non-Newtonian viscosity. Non linear visco-plastic fluid behaviour has been described in terms of non-Newtonian viscosity for investigating mudflows by, among others researchers, LAIGLE & COUSSOT (1997), LAIGLE *et alii* (2007) and RODRIGUEZ-PAZ. & BONET (2003), the last two papers also based on SPH approach. A non-Newtonian rheology description has also been proposed by JOP *et alii* (2006) for modeling dry dense granular flows.

The constitutive law used throughout the paper to simulate the behaviour of a mudflow, assumed as incompressible, is the Herschel-Bulkley law, modified by PAPANASTASIOU (1987) in order to regularize the viscosity that, otherwise, would diverge to infinity for strain rate approaching zero:

$$\eta_p = \left[K\sqrt{2\mathrm{Tr}\left(\underline{\underline{\boldsymbol{\varepsilon}}}^2\right)}^{(n-1)} + \frac{\tau_c}{\sqrt{2\mathrm{Tr}\left(\underline{\underline{\boldsymbol{\varepsilon}}}^2\right)}} \right] \cdot \left\{ 1 - \exp\left[-B\sqrt{2\mathrm{Tr}\left(\underline{\underline{\boldsymbol{\varepsilon}}}^2\right)} \right] \right\}$$

$$\underline{\underline{\boldsymbol{\tau}}} = 2\eta_p \cdot \underline{\underline{\boldsymbol{\varepsilon}}} \quad \text{if } \sqrt{\mathrm{Tr}\left(\underline{\underline{\boldsymbol{\tau}}}^2\right)/2} > \tau_c \tag{3}$$

$$\underline{\underline{\boldsymbol{\varepsilon}}} = \underline{\underline{\mathbf{0}}} \quad \text{if } \sqrt{\mathrm{Tr}\left(\underline{\underline{\boldsymbol{\tau}}}^2\right)/2} \leq \tau_c$$

Where η_p is the local regularized dynamic viscosity of the fluid; τ_c is the yield stress; K is called the 'liquid consistency'; n is called the 'power law index'; $\underline{\underline{\boldsymbol{\varepsilon}}}$ is the strain rate tensor.

In this paper $\underline{\underline{\boldsymbol{\varepsilon}}}$ and the vorticity tensor $\underline{\underline{\boldsymbol{\omega}}}$ are computed from the linear terms of Taylor expansion of velocity in space:

$$\varepsilon_{ij} = \frac{1}{2}\left(\frac{\partial \underline{\mathbf{v}}_i}{\partial x_j} + \frac{\partial \underline{\mathbf{v}}_j}{\partial x_i}\right) \qquad \omega_{ij} = \frac{1}{2}\left(\frac{\partial \underline{\mathbf{v}}_i}{\partial x_j} - \frac{\partial \underline{\mathbf{v}}_j}{\partial x_i}\right) \tag{4}$$

The physical meaning of the yield stress is immediate, representing the stress threshold below which the fluid starts to behave like a rigid body. The parameter B (equal to 10 [s] for all the simulations discussed in this paper) is related to the maximum viscosity returned by the regularization when the strain rate is zero. In this case, the maximum viscosity value is given by: $\eta_{max} = B \cdot \tau_c$. It can be seen from eq. (3) that the regularized and the real viscosities of the model differ significantly from one another only at low values of deformation rates which, in the selected test case, occur only during the first instants of the flow, immediately after the sluice gate is released. Therefore, the B parameter is expected to have a non negligible influence only during the very first instants of the motion. Its value has however been chosen high enough in order to not significantly affect the computed arrival times of the front at the gauges, but small enough to avoid prohibitively small time steps. Furthermore, to quantify the irrotationality of the flow regime, the irrotationality index Irr is introduced as the ratio between the particles average of strain tensor modulus $\| \underline{\underline{\varepsilon}} \|$ and the particles average of the velocity gradient modulus $\| \nabla \underline{\mathbf{v}} \|$. It is easy to show, after straightforward calculations, that $\| \nabla \underline{\mathbf{v}} \| = \sqrt{\| \underline{\underline{\omega}} \|^2 + \| \underline{\underline{\varepsilon}} \|^2}$.

Thus:

$$Irr = \frac{\| \underline{\underline{\varepsilon}} \|}{\| \nabla \underline{\mathbf{v}} \|} \equiv \sqrt{\frac{\| \underline{\underline{\varepsilon}} \|^2}{\| \underline{\underline{\omega}} \|^2 + \| \underline{\underline{\varepsilon}} \|^2}} \tag{5}$$

From eq. (5), if the flow is purely irrotational, then: $\| \underline{\underline{\omega}} \| = 0$ and Irr = 1, while if the flow is purely rotational $\| \underline{\underline{\varepsilon}} \| = 0$ and consequently Irr = 0. It is worth noticing that this kind of index could also be indicative of the occurrence of turbulence phenomena, despite the fact that this kind of phenomena have not yet been introduced in our research code.

OVERVIEW OF THE SPH METHOD

The SPH method is a numerical technique that was initially developed during the 1970s to solve astrophysical problems (MONAGHAN, 2005). It is a fully meshless particle method that is easy to code. Its meshless and Lagrangian nature makes it very attractive for solving fluid flow problems where free surface boundary conditions and large strain rates are involved. The computational domain is filled with particles carrying flow field information (e.g. pressure, velocity, density) and capable of moving in space. Particles are the computational frame used in the method to solve the flow describing PDEs, given that a grid or a mesh to calculate spatial derivatives is not needed. We shall refer to 2D cases throughout the rest of the paper, even though all the assumptions and results can be extended to a 3D case with little effort. The key idea on which the method is based is the well-known use of a convolution integral with a Dirac delta function to reproduce a generic function f ($\underline{\mathbf{x}}$):

$$f(\underline{\mathbf{x}}) = \int_D f(\underline{\mathbf{x}}') \cdot \delta(\underline{\mathbf{x}} - \underline{\mathbf{x}}') d\underline{\mathbf{x}}' \tag{6}$$

In the SPH method, the Dirac function is replaced by a "bell-shaped" kernel function W (it 'mimics' the Dirac delta function), and the generic function f ($\underline{\mathbf{x}}$) is reproduced with a convolution integral that, in a discrete framework, takes the form of a summation over particles:

$$f(\underline{\mathbf{x}}_i) = \sum_{j=1}^{n} f(\underline{\mathbf{x}}_j) \cdot W(| \underline{\mathbf{x}}_i - \underline{\mathbf{x}}_j |) \cdot \Delta A_j \tag{7}$$

Where: $\underline{\mathbf{x}}_i$ and $\underline{\mathbf{x}}_j$ represent the *i*-th and *j*-th particle positions in the given frame of reference; ΔA_j represents the tributary area (or volume in a 3D case) associated with particle *j*-th; summation is extended to all the particles located within the support domain of particle *i*-th. The kernel function is chosen to be non negative, even and with a support domain Ω_x (usually circular) whose radius is a multiple of a length h, named *smoothing length*. The kernel function is zero outside the support domain and the smoothing length serves as a scaling parameter for its arguments. It also has the property of converging to the Dirac function as the smoothing length approaches zero.

The kernel that has been used for the simulations in the present work is the 'C4' (quartic) Wendland kernel (WENDLAND, 1995). Such kernel has good smoothness properties and has also been used previously by MONAGHAN & KAJTAR (2009). Its expression in a 2D case is as follows:

$$W(| \underline{\mathbf{x}} - \underline{\mathbf{x}}' |, h) = \frac{7}{64 \pi h^2} \cdot \begin{cases} (1 + 2R)(2 - R)^4 & \text{for } 0 \le R < 2 \\ 0 & \text{for } R \ge 2 \end{cases} \tag{8}$$

$$R = |(\underline{\mathbf{x}} - \underline{\mathbf{x}}')| / h$$

where ($|\underline{\mathbf{x}} - \underline{\mathbf{x}}'|$) is the ratio between particle distances and smoothing length h. For simplicity, hereafter, the kernel function will be expressed with W ($\underline{\mathbf{x}} - \underline{\mathbf{x}}'$). Smoothing length in SPH, playing a similar role as grid spacing in finite differences or finite volumes method, is the reference length upon which spatial derivatives are interpolated. Different choices are available throughout the related literature. For all the simulations performed and then discussed in this paper, an evolving in time smoothing length h_i, related to each 'i' particle, was calculated by the following ordinary differential equation (BENZ, 1988):

$$\frac{dh_i}{dt} = \frac{h_i}{N_d} \nabla \cdot \underline{\mathbf{v}}_i \qquad h_{i,t=0} = \varepsilon \cdot dp \tag{9}$$

Where $N_d = 2$ for 2D simulations, ε is a non dimensional coefficient, typical ranging between 1.0 and 1.4, dp is the initial fluid particles spacing (tab. 3). For the simulations discussed in this paper, ε = 1.3 was given.

It is possible to obtain the expression for the SPH approximation of a function gradient by writing the convolution integral of the function with the kernel and by using the Gauss-Green formula:

$$\begin{aligned} \nabla f(\underline{\mathbf{x}}) &= \int_{\Omega_x} \nabla' f(\underline{\mathbf{x}}') \cdot W(\underline{\mathbf{x}} - \underline{\mathbf{x}}') \, d\underline{\mathbf{x}}' = \\ &= \int_{\partial\Omega_x} f(\underline{\mathbf{x}}') \cdot W(\underline{\mathbf{x}} - \underline{\mathbf{x}}') \cdot \underline{\mathbf{n}} \, dS - \int_{\Omega_x} f(\underline{\mathbf{x}}') \cdot \nabla' W(\underline{\mathbf{x}} - \underline{\mathbf{x}}') d\underline{\mathbf{x}}' \end{aligned} \tag{10}$$

Where: dS is the boundary surface (a line in 2D and a surface in 3D); ∇' means the gradient respect to the

variable $\underline{\mathbf{x}}'$. If the support domain boundary is fully contained within the computational domain (internal particle), then the first integral of the right side of the eq. (10) vanishes as the kernel $W(\underline{\mathbf{x}} - \underline{\mathbf{x}}')$ is zero on the kernel support domain boundary (KSDB) and outside of it. On the other hand if the KSDB intersects the boundary of the computational domain (particles close to the boundaries), the term does not vanish as the integral must be evaluated on the computational support domain boundary, where the kernel is not vanishing. However it is common practice to neglect this term in any case. In order to compensate for the consequent error, the use of boundary or ghost particles has been proposed (MORRIS *et alii*, 1997; MONAGHAN & KAJTAR, 2009). Another case when the term can be zero is when the support domain is truncated by the computational domain boundaries but there exists a boundary condition forcing the function $f(\underline{\mathbf{x}})$ to vanish on boundaries (it may be the case when $f(\underline{\mathbf{x}})$ represents a velocity and a no-slip condition has to be enforced on the computational domain boundaries). If the first term of the RHS of eq. (10) is zero, then the SPH approximation of $f(\underline{\mathbf{x}}_i)$ gradient, related to the i-th particle, takes the following form in a discrete framework:

$$\nabla f(\underline{\mathbf{x}}_i) = -\sum_{j=1}^{n} f(\underline{\mathbf{x}}_j) \cdot \nabla_j W(\underline{\mathbf{x}}_i - \underline{\mathbf{x}}_j) \cdot \Delta A_j \tag{11}$$

There are consistency conditions that the kernel has to satisfy in order to correctly reproduce continuous field functions up to a certain order of accuracy. These are related to the kernel moments and should be satisfied both in the continuous and in the discrete frameworks. A common drawback in SPH is that while such conditions may be satisfied in the continuous by the kernel, they are not satisfied in the discrete framework due to disorder in particles positions. More details can be found in LIU & LIU (2003) and in LIU & LIU (2006). In summary, numerical applications of SPH share these common features:

– the equations describing the continuum motion are written in Lagrangian form, by using Lagrangian instead of Eulerian time derivatives;

– the spatial gradients involved in the PDEs are discretized over the particles, by using a SPH approximation;

– time integration of variables is performed particlewise, usually by using an explicit time stepping method;

– particle positions are evolved in time, according to the velocity of each particle.

SPH DISCRETIZATION TECHNIQUE

In this section, the SPH numerical approaches, according to which our research code was developed, are briefly introduced.

MAIN EQUATIONS (CONTINUITY AND MOMENTUM)

There are many references where it is possible to find details on how fluid flow governing equations can be effectively discretized into SPH equations. Of the many, we indicate TAKEDA *et alii* (1994), LIU *et alii* (2003), MONAGHAN (2005) and LIU & LIU (2010). The SPH discretization of the mass conservation equation, eq. (1), used in the paper is based essentially on the following equation:

$$\frac{D\rho_i}{Dt} = \sum_{j=1}^{n} m_j \cdot \underline{\mathbf{v}}_{ij} \bullet \nabla_i W_{ij} \tag{12}$$

Where: m_j represents the particle mass; $\underline{\mathbf{v}}_{ij} = \underline{\mathbf{v}}_i - \underline{\mathbf{v}}_j$ is the difference between the interacting particle velocity. A widely used SPH discretization of the momentum equation eq. (2), in the case of Newtonian and non Newtonian viscous fluids, is as follows:

$$\begin{aligned} \frac{D\,\underline{\mathbf{v}}_i}{Dt} &= \underline{\mathbf{f}}_i - \sum_{j=1}^{n} m_j \cdot \left(\frac{p_i}{\rho_i^2} + \frac{p_j}{\rho_j^2} \right) \cdot \nabla_i W_{ij} + \\ &+ \sum_{j=1}^{n} m_j \cdot \frac{8\eta_{ij}}{\rho_i \rho_j} \cdot \frac{\underline{\mathbf{v}}_{ij} \bullet \underline{\mathbf{r}}_{ij}}{|\underline{\mathbf{r}}_{ij}|^2} \cdot \nabla_i W_{ij} \end{aligned} \tag{13}$$

Where: $\underline{\mathbf{r}}_{ij} = \underline{\mathbf{r}}_i - \underline{\mathbf{r}}_j$ represents the difference between the interacting particle position; η_{ij} is a symmetrised dynamic viscosity between interacting particles, such that $\eta_{ij} = \eta_{ji}$. Usually, a symmetrised expression for the smoothing lengths of each pair of interacting particles in summations is used when calculating the kernel gradient: $h_{ij} = (h_i + h_j)/2$. If this is the case, it can be shown that particles exchange equal and opposite forces, making eq. (13) capable of conserving the linear momentum of the particles system. In the paper, the following expression has been used for symmetrised viscosity:

$$\eta_{ij} = \frac{2\eta_i \eta_j}{\eta_i + \eta_j} \tag{14}$$

The term on the right hand side of eq. (13) involving the symmetrised viscosity represents the deviatory stress tensor divergence. Such an expression has been proposed by CLEARY (1998) and MONAGHAN (2005) and also accounts for the presence of spatial gradients in viscosity. It is possible to prove that eq. (13) implicitly includes a bulk viscosity coefficient ξ, which is equal to 5/3 times the dynamic shear viscosity η, $\xi = (5/3)\,\eta$. Proof of this for a Newtonian viscous fluid can be found in ESPANOL *et alii* (2003).

It is a common practice in SPH (MONAGHAN, 2005) to approximate an incompressible flow with a weakly compressible one (see next sub-section for more details). This results in slight density variations and therefore in velocity fields with low but not zero values of divergence. Therefore, the bulk viscosity introduced by eq. (13) acts on the motion of particles through the velocity divergence term by dampening volume variations: this has a low influence on the simulations results but these issues will be more deeply investigated in further papers.

A possible alternative to eq. (13) is the one of directly calculating the total stress tensor from eq. (11) and to use the following SPH approximation for its divergence:

$$\frac{D\underline{\mathbf{v}}_i}{Dt} = \underline{\mathbf{f}}_i + \sum_{j=1}^{n} m_j \cdot \left(\frac{\underline{\underline{\boldsymbol{\sigma}}}_i}{\rho_i^2} + \frac{\underline{\underline{\boldsymbol{\sigma}}}_j}{\rho_j^2} \right) \bullet \nabla_i W_{ij} \tag{15}$$

Another possible formulation for the viscous term was proposed by MORRIS *et alii* (1997) for the simulation of incompressible viscous flows at low Reynolds num-

bers. By using Morris viscous term, the SPH formulation for the momentum equation is as follows:

$$\frac{D\underline{\mathbf{v}}_i}{Dt} = \underline{\mathbf{f}}_i - \sum_{j=1}^{n} m_j \cdot \left(\frac{p_i}{\rho_i^2} + \frac{p_j}{\rho_j^2}\right) \cdot \nabla_i W_{ij} + \\ + \sum_{j=1}^{n} \frac{(\eta_i + \eta_j)(\underline{\mathbf{r}}_{ij} \bullet \nabla_{\mathbf{r}_{ij}} W_{ij})}{|\underline{\mathbf{r}}_{ij}|^2 \rho_i \rho_j} m_j \underline{\mathbf{v}}_{ij} \tag{16}$$

The equation (16) exactly represents the viscous term of the momentum equation up to the 2nd order. In this paper the following small modification of the last term of Morris momentum eq. (16) was implemented and the consequent numerical results were compared and discussed:

$$\frac{D\underline{\mathbf{v}}_i}{Dt} = \underline{\mathbf{f}}_i - \sum_{j=1}^{n} m_j \cdot \left(\frac{p_i}{\rho_i^2} + \frac{p_j}{\rho_j^2}\right) \cdot \nabla_i W_{ij} + \\ + \sum_{j=1}^{n} \frac{2\eta_i \eta_j}{(\eta_i + \eta_j)} \frac{(\underline{\mathbf{r}}_{ij} \bullet \nabla_{\mathbf{r}_{ij}} W_{ij})}{|\underline{\mathbf{r}}_{ij}|^2 \rho_i \rho_j} m_j \underline{\mathbf{v}}_{ij} \tag{17}$$

From the above discussion it is clear how the Lagrangian nature of the method makes it very easy to reproduce free surface flows. The free surface boundary condition is automatically incorporated into all the proposed versions of momentum equation, eqs. (15) to (17). When the *i*-th labeled particle in the equations is located close to the free surface, summations are truncated as its support domain is incomplete. A fairly natural way to represent a free surface boundary condition would be the one of filling the empty parts of the support domain with particles having zero stresses and the same velocity as the particles on the free surface: if this procedure were to be followed then the results would be the same as truncating the summations in eqs. (15) to (17) as such particles would provide no contributions ($\underline{\mathbf{v}}_{ij} = \underline{\mathbf{v}}_i - \underline{\mathbf{v}}_j = 0$). That is indeed the main reason why the use of a Lagrangian approach was investigated in the present work to reproduce mudflow dam break problems. Another advantage of SPH is that it can be easily adaptable to reproduce different rhelogical behaviours: eqs. (15) to (17) can be used to simulate the behaviour of every non-Newtonian fluid, provided the correct values of viscosity are employed in the equations.

Artificial Compressibility

The simulation of an incompressible flow requires the solution of a Poisson equation for the pressure, which often leads to an increase of the computational time. Therefore, it is more practical to approximate the incompressible medium with a weakly compressible one, thus allowing the calculation of the pressure from the density with a stiff equation of state which introduces an artificial compressibility into the fluid. It can be shown that density variation is proportional to the square of the Mach number (Monaghan, 1994). If an artificial equation of state where the speed of sound is greater than the bulk velocity of flow is used, then it is possible to keep density variations as low as desired. Thus the selected artificial equation of state used in this paper is as follows:

$$p_i = c^2(\rho_i - \rho_0) \equiv \left(\frac{\sqrt{g \cdot H}}{M}\right)^2 (\rho_i - \rho_0) \tag{18}$$

where H is the maximum initial dam height and p_i is the pressure associated to the *i*-th particle; c is the artificial speed of sound; M is the selected value (in input) of Mach number; ρ_0 is the reference density of the fluid at zero pressure. The sound speed value is the same for all particles: this is due to the assumption that the equation of state being a linear function of density.

Numerical simulation of a fast front flow

Another important numerical issue is encountered in the computation of shocks waves, common phenomena in hydrodynamic problems, especially when low dissipation occurs. This is strictly related to the hyperbolic nature of the governing equations. A shock is very similar to discontinuity propagating within the flow or already at the boundary front of the flow, as it physically is a very sharp variation occurring at a length scale much smaller than usual numerical resolutions. Numerical methods, including SPH, develop unphysical oscillations around the fronts of shocks, like a front of a fast flow, unless some special treatment is adopted. Good numerical treatment of shocks is able to dampen oscillations and to restore correct values ahead and beyond the shock front; a correct simulation of front sharpness is still very difficult to achieve as it would require an excessive spatial resolution. A common approach of numerical methods is that of dissipating the kinetic energy of the shocked region into heat by adding an artificial viscosity term to the momentum equation. Monaghan & Gingold (1983) and later Monaghan (1994) also adopted this approach, adding an artificial viscous term to the momentum equation. They devised an expression capable of increasing entropy, in order to provide dissipation to the system:

$$\Pi_{ij} = -\nu \frac{\underline{\mathbf{v}}_{ij} \bullet \underline{\mathbf{r}}_{ij}}{|\underline{\mathbf{r}}_{ij}|^2}; \nu = \frac{\overline{h}_{ij}}{\overline{\rho}_{ij}} \left(\alpha \cdot c - \beta \frac{\overline{h}_{ij} \underline{\mathbf{v}}_{ij} \bullet \underline{\mathbf{r}}_{ij}}{|\underline{\mathbf{r}}_{ij}|^2}\right) \tag{19}$$

where: α and β are non dimensional coefficients, while the over line sign represents the arithmetic average between quantities. Its stabilising mechanism mainly relies on the fact that it produces an attractive force when two particles are receding from each other and vice-versa. It is possible to use artificial viscosity for compression shocks only and not for rarefaction shocks by turning it off if $\underline{\mathbf{v}}_{ij} \bullet \underline{\mathbf{r}}_{ij} > 0$ (receding particles).

Rusanov Flux

The equations discussed so far are usually referred to as a 'standard' SPH scheme. This formulation, continuity equation (12) in particular, is like a centered finite difference scheme, centered on the location of particle *i*-th. To focus on the idea, let's consider a 1D inviscid fluid flow situation. The spatial gradients at particle *i*-th are evaluated from the values of the velocity of particles standing on the left and on the right of the particle itself through the kernel gradient. It can be shown that this scheme is non monotone and it is reasonable to infer that this could be the reason why standard SPH simulations produce unphysical high frequency density oscillations (Ferrari *et alii*, 2009). On the other hand, the momentum equation formulation of the standard scheme is not very diffusive and works well in computing particle posi-

tions. FERRARI *et alii* (2009) suggest therefore a correction to the continuity equation that both creates a density monotone scheme and leaves substantially unaffected the low diffusivity of the original SPH formulation, by adding a flux term devised from the Rusanov flux (VILA, 1999; TORO, 2009):

$$\frac{D\rho_i}{Dt} = \sum_{j=1}^{n} m_j \cdot \underline{v}_{ij} \bullet \nabla_i W_{ij} + \\ + \sum_{j=1}^{n} \frac{m_j}{\rho_j} \cdot c \cdot (\rho_i - \rho_j) \frac{\nabla_i W_{ij} \bullet \underline{r}_{ij}}{| \underline{r}_{ij} |} \qquad (20)$$

A first result is certainly the improved density time evolution, as it is highlighted by the trend of the Rusanov flux line compared to the Standard scheme in fig. 1, obtained performing a dam break flow simulation, as partially discussed in MINATTI & PASCULLI (2010). Conversely a shortcoming of the Rusanov flux is that, analytically, the mass conservation constraint is no longer satisfied since it results, eq. (20), in the addition of a mass diffusion term in the density equation of continuity.

BOUNDARY TREATMENT

Since the gradient formulation given by eq. (11), with symmetric shape function, is used even for fluid particles close to the boundaries, special treatments are required in order to offset the errors introduced by neglecting the terms in the right hand side of eq. (10). In this paper, the Ghost Particles (also Image or Wall particles) approach proposed by MORRIS *et alii* (1997) (see also TAKEDA *et alii* (1994), FERRARI *et alii* (2009) who use point symmetry) was selected, while the Boundary Forces approach by MONAGHAN & KAJTAR (2009) was already explored in the previous paper MINATTI & PASCULLI (2011). In the Morris approach, to enforce boundary conditions, particles also named "image" or "wall particles" with the same viscosity, tensions and pressures of the free particles they interact with, are employed. In MORRIS *et alii* (1997), in order to set no-slip conditions, the following extrapolated 'virtual' boundary particles velocities were given:

$$\underline{v}_{bound} = -\theta \cdot \underline{v}_{free}; \quad \theta = \min(\theta_{max}, 1 + d_w / d_f) \qquad (21)$$

where $\theta_{max} = 1.5$ and d_w, d_f , are, respectively, the normal distance of the involved wall particle and the selected free particle from the boundary. Such velocity for wall particles was then used in the SPH equations. In the Monaghan approach, boundaries have been treated by placing a layer of particles on them. Boundary particles prevent fluid particles from passing through the domain boundaries by exerting a normal force. They also interact with the fluid particles via SPH summations through their viscosity, thus enforcing the no-slip condition. The expression for the boundary forces proposed by Monaghan is:

$$\underline{F}_i = \sum_{j=1}^{n} k \frac{2 m_i m_j}{m_i + m_j} \frac{W_{ij}}{| \underline{r}_{ij} |^2} \underline{r}_{ij} \qquad (22)$$

where: k is a constant having the dimensions of a square velocity ($k = g \cdot H[m]^2[s]^{-2}$, where g = gravity acceleration, H = height of material behind the gate) used to correctly reproduce the bulk forces exerted by the boundaries on the fluid; summation is extended to all the boundary particles located within the support domain of *i*-th fluid particle. It can be shown (MONAGHAN & KAJTAR, 2009), that the above summation gives negligible contribution along the direction parallel to the boundary, making boundary forces being exerted only along the normal direction. It is also a symmetrical formulation, thus conserving the linear momentum of the particles system.

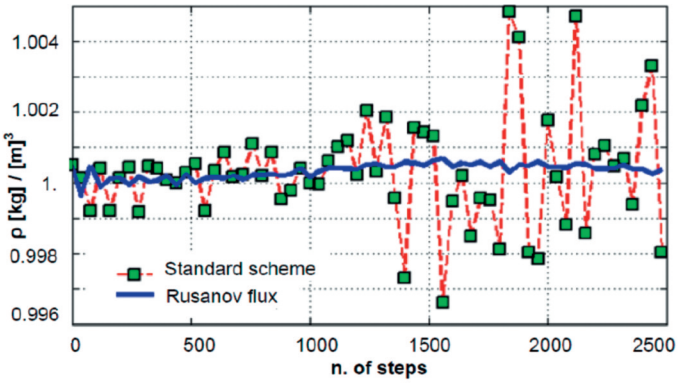

Fig. 1 - Particles-averaged density fluctuations for an inviscid dam break simulation based on both the standard SPH scheme and the scheme with the Rusanov flux terms in the continuity equation.

TIME INTEGRATION

Time integration has been performed by means of a symplectic Verlet scheme, as in KAJTAR & MONAGHAN (2008). The time stepping scheme is explicit and conserves the linear and angular momentum of the particles system. The time step Δt is controlled by a CFL (Courant-Friedrichs, Lewy) condition depending on the artificial speed of sound, the viscous interactions between particles and on the interactions with boundary particles, according to the following equation:

$$\Delta t = CFL \cdot \min\left(\frac{h_{ij}}{c}; \quad 0.1 \frac{\rho_{ij} h_{ij}^2}{\eta_{ij}}; \quad \frac{| \underline{r}_{ij} | - \frac{dp}{\psi}}{\max(| \underline{v}_i |, \sqrt{k})} \right) \qquad (23)$$

Where: the minimum time step value is sought over each couple of interacting particle; $\rho_{ij} = (\rho_i + \rho_j)/2$ is a

TABLE 1

Rheological characteristics and experimental parameters (after LAIGLE & COUSSOT, 1997); Material A; see eq. (3) for the meanings of yield stress, power law and liquid consistency within the Herschel Bulkley rheology.

density (ρ_0)	1410 (kg/m^3)
yield stress (τ_c)	19 (Pa)
power law index (n)	1/3
liquid consistency (K)	3.5 (Pa·s^n)
Flume slope	21 (%)
Initial height of material (measured at the gate)	14 (cm)

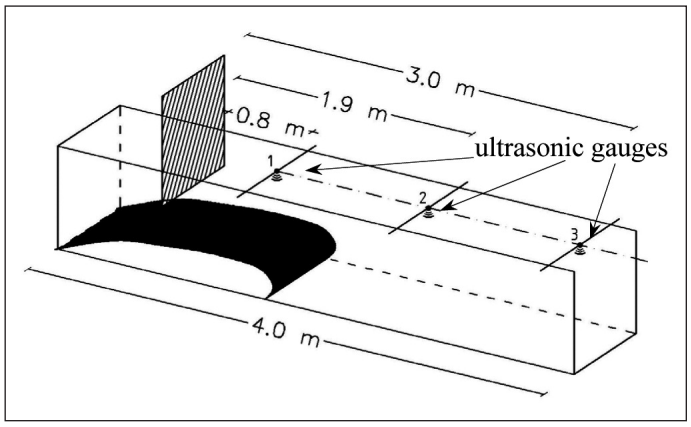

Fig. 2 - 3D sketch of the selected experimental device (freely adapted from LAIGLE & COUSSOT, 1997).

symmetrised density between the pair of interacting particles; dp is the initial fluid particles spacing; ψ is the ratio between the boundary and the fluid particles spacing; the CFL number has been set equal to 0.5; k is the constant defined previously in eq. (22).

FINAL REMARKS

The previous sub sections sought to highlight both the drawbacks and the advantages of using a SPH method to simulate the dam break problem of a mudflow.

In our opinion, the correct tracking of free surface is of crucial importance in order to correctly reproduce the mudflow front advancement in time for the selected kind of problem, and this is the main reason why SPH has been selected. On the other hand, the use of a different method such as finite volumes with volume of fluid approach to track free surface would have probably provided very similar results but at the cost of using a more complicated approach. Another feature of the simulated test case which contributed to the selection of SPH is that heavy deformations in the continuum occur during the flow. Such heavy distortion within a grid-based numerical method framework would have required frequent mesh updates making the simulations very complicated to be handled properly. Finally we would like to point out that while certain parameters need to be calibrated within the method, all of them have a sound physical meaning and their values can be readily set up. Going into detail, a list of parameters pertaining to numerical aspects of SPH are reported below accompanied by commentary:

– Mach number: this is set up in order to have a weak artificial compressibility for the fluid as relative density variations during the flow are proportional to its squared value. It influences the multiplying coefficient in the equation of state and it is usually set up to be lower than 0.3.

– Artificial viscosity coefficients eq. (19): these control artificial energy dissipation at shocks; α is usually set up to be lower than unity, while β, when not equal to zero, is usually around twice α.

– Particle spacing: this is equivalent to grid spacing in grid based methods.

The values used for the parameters indicated above during the simulations are, however, listed in tab. 3, included in the section in which results are discussed. Finally, despite the fact that 3D effects have an influence on the flow mostly through the wall shear, they were excluded at this stage of the study.

SELECTED EXPERIMENTAL TEST

The ability of the selected SPH approaches to correctly reproduce a fast flow has been tested by simulating the experiments performed by LAIGLE & COUSSOT (1997) (L&C). Their experiments consisted of creating a mudflow dam break problem in a laboratory flume, by quickly opening a gate. The experimental setup they used is briefly shown in the fig. 2. After the opening of the gate, the material stored behind it was released and the three ultrasonic gauges, sketched in the picture, recorded the mudflow front heights over time. L&C used water-clay mixtures prepared in the laboratory with different concentrations in order to recreate mudflows.

Herschel-Bulkley rheological parameters, for the mixtures used, were fitted to measurements carried out with a rheometer. The rheological characteristics of one of the experimental mixture utilized by the authors of the tests and also selected for all the simulations discussed in the following paragraphs are summarized in tab. 1.

TABLE 2

Basic simulations features.

Simul. n.	Particles number		Number of time steps
	total (bound.+free)	free	
0	9628	5486	600000
1	9701	5555	500000
2	9701	5555	500000
3	9701	5555	433000
4	17654	11644	1000000
5	9701	5555	500000
6	9701	5555	466000
7	9701	5555	500000
8	17654	11644	1000000
9	9701	5555	371000
10	9701	5555	371000

Furthermore, the authors of the experimental tests modelled the mudflow as a wide channel flow initially at rest: the resulting flow conditions were therefore completely determined by the height of the material stored behind the gate, the flume slope and the material characteristics. They indicated two non dimensional scaling parameters controlling the resulting flow conditions. The values of the scaling parameters in the tests they performed can represent a wide range of real situations at smaller scales (COUSSOT, 1994). In particular, the material we selected, along with the experimental conditions of tab. 1, represent a realistic natural material (with $\rho_0 = 2200$ Kg/m^3, $\tau_c = 900$ Pa, K = 290 Pa s$^{1/3}$) in a 120 m long slope (LAIGLE & COUSSOT, 1997). A field determination of the Herschel-Bulkley rheological parameters of a natural debris flow can be found in COUSSOT *et alii* (1998), even though the values provided for the parameters in that paper are in a slightly different range than those indicated in tab. 1.

CONSIDERATION CONCERNING EXPERIMENTAL DATA

Data on arrival times for the selected test are affected by experimental errors, ranging from ±5 to ±15% and up to ±20% (LAIGLE & COUSSOT, 1997). As a consequence, experimental uncertainties could be large enough to hide possible inaccuracies of the selected numerical models, as indeed is discussed in the cited article. Nevertheless, we tried to devise probabilistic considerations in order to make a comparison between the numerical results and the available data which are affected by experimental errors. Hence, we assume that the real experimental value of debris front arrival time ('at') at the k-th gauge is a random variable $X_{at,k}$ [s], affected by only random errors (as simplified hypothesis), whose probability density function (pdf) is the Gaussian distribution with a mean μ_k equal to the value assessed from experiments by an additional graphical inspection. For Gaussian probability density function (pdf) (JAMES, 2006), the probability Pr (·) for an experimental (random) variable $X_{at,k}$ to be within the numerical range: $\mu_k - \lambda \cdot \sigma_k \le X_{at,k} \le \mu_k + \lambda \cdot \sigma_k$ around the mean μ_k with a standard deviation σ_k is:

$$\Pr\left(\mu_k - \lambda \cdot \sigma_k \le X_{at,k} \le \mu_k + \lambda \cdot \sigma_k\right) = \\ = \frac{1}{\sigma_k \sqrt{2\pi}} \int_{\mu_k - \lambda\sigma_k}^{\mu_k + \lambda\sigma_k} e^{-\frac{\left(X_{at,k} - \mu_k\right)^2}{2\sigma_k^2}} dX_{at,k} \tag{24}$$

From a statistical point of view, the request of including, for comparison purposes, a range of variability of $X_{at,k}$ as wide as possible is obviously desirable. Therefore, from the theory (JAMES, 2006), it is required that $\lambda = 3.29$ at least, in order to satisfy Pr ≥ 99.9%. Then, since the value of the experimental arrival time is realistically affected (from the previous discussion) by an error equal to ±20%, to which here ±5% error is added, reasonably due to the graphics inspection, the value of the standard deviation follows: $3.29 \cdot \sigma_k = 0.25 \cdot \mu_k$ and hence $\sigma_k = 0.076 \cdot \mu_k$. It is important to note that we consider 3 decimal digits for both numerical results and experimental values estimated by the inspections of plots, merely for numerical comparisons purposes. Moreover it is important to discuss certain underlying hypothesis. In fact, the total estimated value of the relative error with respect to the measured arrival time 25% is assumed to be constant. It follows that the assumed absolute spreading concerning measured data, $\sigma_k = 0.076 \cdot \mu_k$, grows over time since μ_k obviously increases. This consequence may be unrealistic, and therefore for the purposes of comparison we explored the assumption that the absolute error assumes the minimum constant value of $0.25 \cdot \mu_1$, where $\mu_1 = 0.431$ (arrival time at the first gauge). At this point the value $X_{num,k}$ of the arrival time, provided by each numerical SPH simulation, is assimilated to a possible value that the random variable $X_{at,k}$, actually measured for the k-th gauge, may assume. Then, to evaluate how probable $X_{num,k}$ is regarding the assumed distribution values (μ_k, σ_k) associated to the actual measured arrival time $X_{at,k}$, a variable which saves the features of the given distribution and whose deviation from the most probable arrival time value μ_k is weighted with respect to the statistical dispersion σ_k, is given: $z_k = (X_{num,k} - \mu_k)/\sigma_k$. Of course, the higher is the numerical value of z_k the less probable the value $X_{num,k}$ will be. Thus, in order to acquire indications concerning the performances of different selected SPH approaches through their reciprocal comparison, 'Performance Index' $I_{N,k}$ is considered. $I_{N,k}$ is the ratio between the value of the Normal probability density distribution N (μ_k, σ_k, z_k), that is calculated for $z_k \neq 0$, and N (μ_k, σ_k, 0), calculated for $z_k = 0$ ($X_{num,k} \equiv X_{at,k} = \mu_k$). Such index aims at normalization with respect to the maximum pdf possible value and is introduced for each gauge arrival time and for each simulation. Its expression, also considering the previous assumptions, is as follows:

$$I_{N,k} = \exp\left\{-\frac{(X_{num,k} - \mu_k)^2}{2 \cdot (0.076 \cdot \mu_k)^2}\right\} \tag{25}$$

Besides the uncertainty on arrival times, significant experimental errors also affect the values of the Herschel-Bulkley rheological parameters characterizing the fluid used. Preliminary calculations, not reported in this paper, show that the selection of the numerical values of parameters such as τ_c and K in some way affect the prevision of arrival time, in particular at gage 3. Subsequent papers will also focus on acquiring more quantitative insights on how experimental uncertainties, related to the principal parameters of the selected laws, may affect the selection of the most appropriate SPH modelling to study this type of debris flow.

NUMERICAL SIMULATIONS

In our SPH simulations, particles were stored behind the gate and a layer of boundary particles was placed to simulate the closed gate at the initial time step. Particles were initially stored in a uniform lattice according to their spacing and were given an initial density value (see tab. 1). More than 30 numerical simulations were carried out, but only 11 of them are discussed in this paper. In tab. 2 some of the basic characteristics of the simulations are reported, regarding the total number of particles (boundary or virtual particles and free particles) and the number of time-steps. Before releasing the sluice gate and initiating the motion, a hydrostatic pressure distribution was built up into the particles: this was achieved by letting particles rearrange their positions under the combined effect of pressure gradients and gravity. In this phase, viscous terms were taken out of the momentum equation and replaced by a damping term (see also MONAGHAN, 1994), proportional to particle velocity. After hydrostatic pressure distribution was reached the gate was released and the usual terms in the momentum equation were restored. The number of damped time steps necessary to reach the hydrostatic pressure distributions ranged from 3000 (low-res simulations) to 20000 (high-res simulations). Subsequently, the gate opening was simulated by removing the layer of boundary (or wall) particles placed on it, thus releasing the mudflow. The artificial Mach number was set to a value ranging from 0.03 up to 0.2 (tab. 3). Another important parameter is the initial particle spacing dp (tab. 3), which plays the same role as the grid spacing in finite differences schemes. Generally, a decrease in the spacing (increasing the number of particles) improves accuracy and reduces numerical dissipation but, as will be discussed in the following paragraphs, it is not always enough. As the physics of the flow is dominated by viscosity, the choice of the SPH discretization for the momentum equation plays an important role.

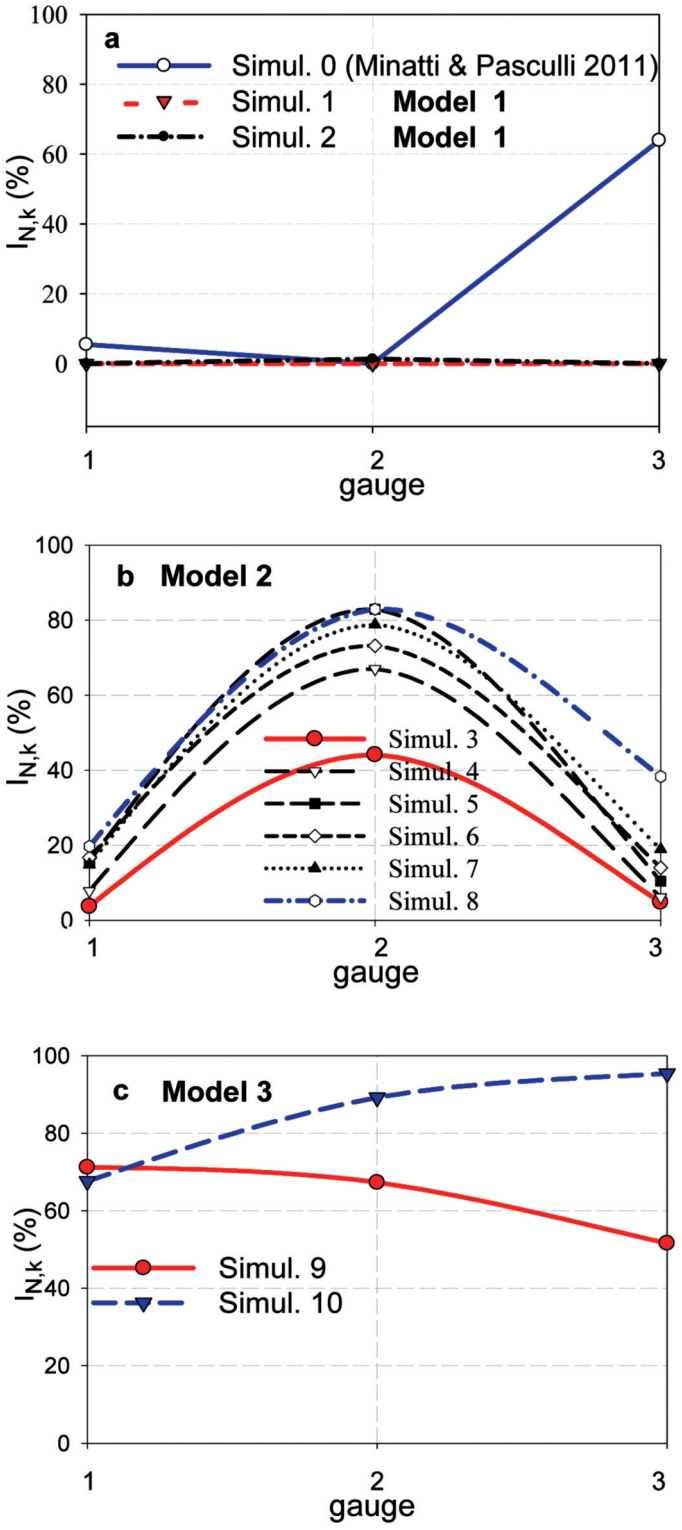

Fig. 3 - Trend of the numerical models performances compared to the experimental data.

Main features of the different selected SPH formulations

An important distinctive feature of an SPH model is related to how the selected approach simulates the viscosity interaction between particles. For this reason the performances of three different approaches, that can in principle correctly simulate a viscous non-Newtonian Herschel-Bulkley fluid, were explored. The main features of the proposed models, whose proof and discussions will form the content of other papers to be submitted, are briefly summarized below.

Model-0

Only one simulation (Simulation 0) belongs to Model-0 since it was already discussed in Minatti & Pasculli (2011) and is reported in this paper for the sake of completeness. The main related characteristics are: dp = 3. mm, eq. (15) as momentum equation, no Rusanov Flux terms in continuity equation, Mach number equal to 0.2, Monaghan boundary force, eq. (22) and, finally, no artificial viscosity terms eq. (19) (tab. 3). Moreover:

– it is a direct calculation of the stress tensor and its divergence for the momentum equation;
– it conserves linear momentum of the SPH particles system;
– it theoretically describes the behavior of an incompressible fluid, as no velocity divergence related terms appear in the momentum equation;
– k coefficient for boundary particles calculation, related to eq. (22) (already discussed), was set up and then decreased during the flow by using an average value for the front height instead of H.

Model-1

– it is a direct calculation of the stress tensor and its divergence for the momentum equation, eq. (15);
– it conserves linear momentum of the SPH particles system;
– it theoretically describes the behavior of an incompressible fluid, as no velocity divergence related terms appear in the momentum equation;
– artificial viscosity terms, from eq. (19), are added to the momentum equation, eq. (15).
– Morris wall particles are used.

Model-2, Monaghan and Cleary approach

– it envisages eq. (13) for linear momentum;
– it conserves both linear and angular momentum of the SPH particles system;
– it has C_0 consistency in the calculation of shear rates (exact calculation of the gradient in the case of a constant velocity field);
– it is transparent to rigid rotations (provides zero viscous forces between particle that are rigidly rotating one with respect to another);
– it is an analytically exact representation up to the second order of the viscous terms in the momentum equation, for a compressible non-Newtonian viscous fluid whose bulk viscosity ξ is 5/3 of its shear viscosity η. Up to the 2^{nd} order, errors are therefore only due to particle disorder.
– Morris wall particles are used.

Model-3, Morris approach

– it envisages eq. (17) for linear momentum;
– it conserves linear momentum of the SPH particles system;
– it has C_0 consistency in the calculation of shear rates (exact calculation of the gradient in the case of a constant velocity field);

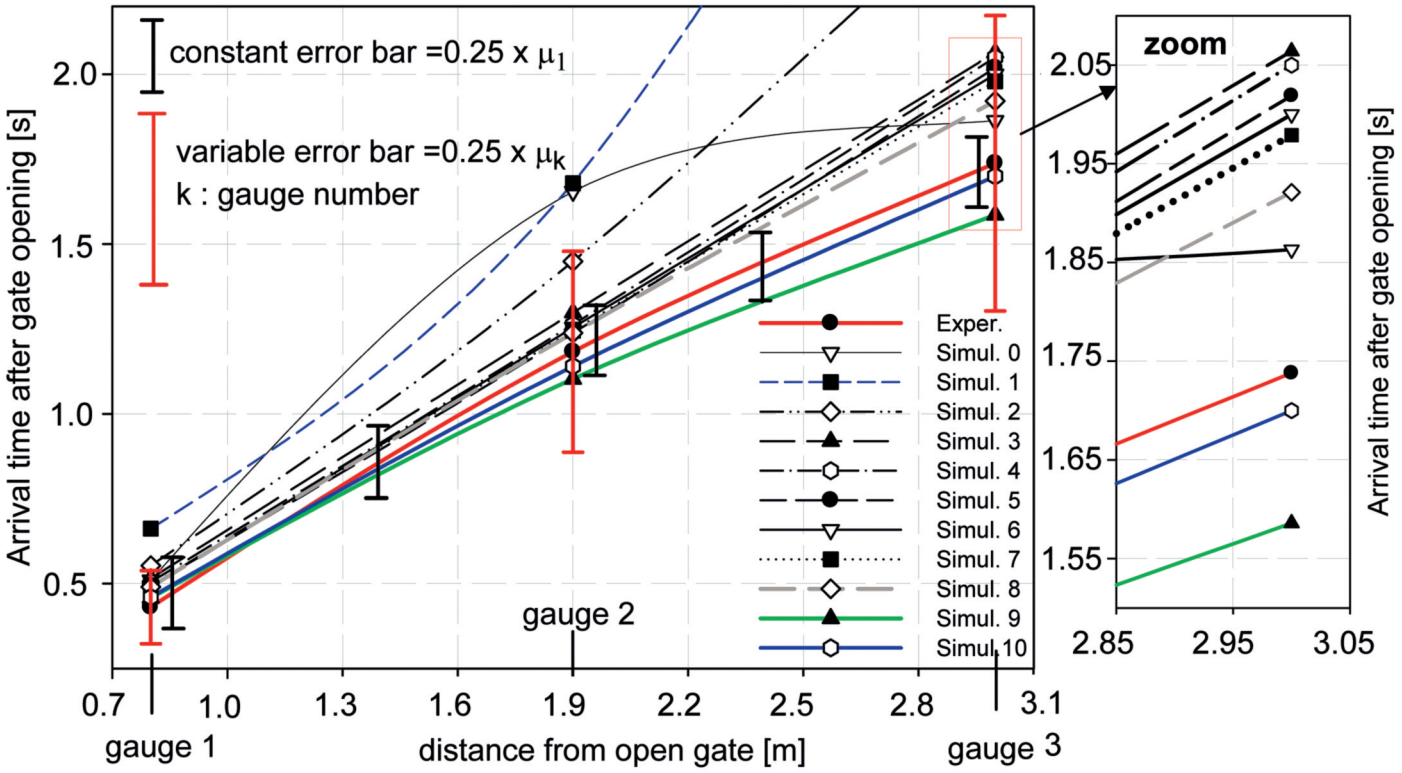

Fig. 4 - Comparison between numerical arrival times and experimental data.

– it is an analytically correct representation up to the second order of the viscous terms in the momentum equation for a compressible non-Newtonian viscous fluid, whose bulk viscosity ξ is 2/3 of its shear viscosity η, provided that the flow field is irrotational (proof to be provided in future papers). An initial consideration is that the main drawback of Model-2 and 3 is the one of introducing a bulk viscosity, which is not present in the original Herschel-Bulkley rheology. However, if the simulated fluid has a low compressibility, it could be assumed that the effect of this artificially induced viscosity is negligible.

– Morris wall particles are used.

RESULTS DISCUSSION

Results related to each model are discussed. Tab. 3 summarizes the main features of the simulations and makes comparisons between the arrival times of the front, obtained numerically, and the data measured at three different points (gauges), placed at the positions indicated in fig. 2. For each one of the three SPH models, fig. 3 shows the graph of the index $I_{N,k}$ which is indicative, according to the previous discussion, of how high the probability is that the numerical result is close to the real value of the arrival time measured from experiments. Fig. 4 shows the direct comparison between numerical arrival times and experimental data, estimated within the range indicated by constant vertical bars and variable error bars. The rationale of fig. 3 is related to statistical considerations, while fig. 4 is more connected to the physical features of the phenomena, as, for example, the acceleration of debris front. The extrapolated front heights below the locations of the ultrasonic gauges used in the experiments of Laigle & Coussot (1997) and the numerical results of some of the simulations belonging to Models 2 and 3, have been compared. Numerical front heights have been calculated by measuring the thickness of the layer of particles passing below the gauges locations. A brief discussion related to each implemented models follows.

Model-0

In fig. 5 the time plot of the simulated front heights at the locations of the three gauges, named Simulation 0 (Minatti & Pasculli, 2011), is reported. Even though heights are well captured, this kind of SPH simulation is still affected by a degree of numerical diffusion, as the calculated front's velocity is lower than the experimental data as it is clear from the numerical results related to the first two gauges in fig. 3a and fig. 4.

Moreover, from the numerical arrival time at the third gauge, displayed in fig. 4, it is clear that the numerical front experiences unphysical accelerations on the last part of the transitory. For this reason, the good result related to the final part of the transitory, reported in fig. 3a for $I_{N,k}$ relating to Simulation 0 is obviously misleading. The high diffusivity of the model is probably due to the lack of consistency (neither 0th order) of the formulation employed for the momentum equation: unphysical viscosities are probably added to those provided by the model due to truncation errors in particle approximations of stress tensor divergence. Another drawback of the problem is represented by the use of Monaghan boundary particles to model the flume bottom: they seem to exert excessively high forces on fluid particles with the outcome that the

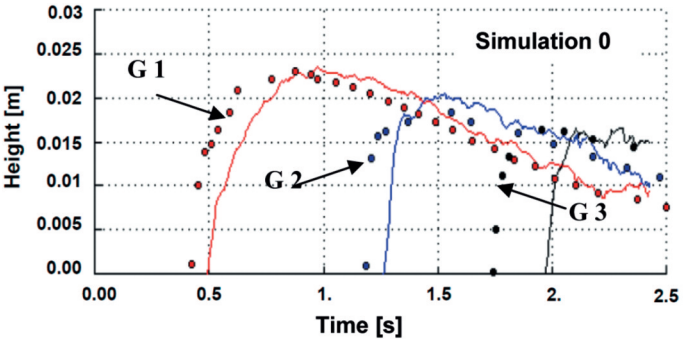

Fig. 5 - Time plot of the simulated front heights at the locations of gauge 1 (G 1), gauge 2 (G 2) and gauge 3 (G 3). Experimental measurements at the three gauges are represented by dots, while numerical results are shown with solid lines.

latter are too detached to the bottom of the flume for viscous interactions to be properly modelled.

Model-1

Model-1 differs from Model-0 in the use of artificial viscosity, eq. (19) and in the use of Morris wall particles instead of Monaghan boundary particles. Simulation 1 differs from Simulation 2 (both using SPH Model-1) in the value of parameter α in eq. (19) (tab. 3). The outcomes of both Simulation 1 and Simulation 2, displayed in fig. 3a and fig. 4, show an excessively diffusive behavior of the flow. The reasons for the still too high diffusivity of the model are the same as for model 0.

The conclusion is that Model-1 is not suitable for the case under study.

Model-2

Good performances have been observed applying this model. Nevertheless, numerical viscosity, related to the spatial resolution (spacing of particles) and a bulk viscosity due to the analytical structure of the model are introduced by the numerical approach. The statement that the errors introduced by the Model-2 are due to numerical viscosity, is confirmed by comparison (tab. 3 and fig. 3b) between the results of Simulation 3 and Simulation 4: in the latter a lower initial spacing of particles 'dp' was adopted (tab. 3) with a consequent increase of the performance index $I_{N,k}$ (fig. 3b). The increase in resolution reduces the effects of numerical viscosity that is introduced by the truncation error in the discretization of gradients, anticipating the arrival times of the front of the debris flow at the gauges. Another possibility for the improvement of Model-2 is represented by the reduction of the effects of bulk viscosity introduced by the model. This can be done by simulating a less compressible fluid, that is, lowering the Mach number.

TABLE 3

Main simulations and numerical results features.

Main simulations characteristics						GAUGE 1		GAUGE 2		GAUGE 3	
						arriv. [s]	$I_{N,k}$ (%)	arriv. [s]	$I_{N,k}$ (%)	arriv. [s]	$I_{N,k}$ (%)
Experimental test						0.431		1.183		1.738	
simul. n.	artificial viscosity	density	momentum equation	dp (mm)	Mach						
0	=	=	eq. 15	3.	0.2	0.510	5.46	1.655	$<10^{-1}$	1.863	63.9
1 model-1	α=0.1; β=0. eq.19	=	eq. 15	2.9	0.2	0.662	$<10^{-1}$	1.679	$<10^{-1}$	3.610	0.0
2 model-1	α=0.05; β=0. eq.19	=	eq. 15	2.9	0.2	0.553	$<10^{-1}$	1.449	1.3	2.571	0.0
3 model-2	=	=	eq. 13; 14	2.9	0.2	0.515	3.7	1.298	44.1	2.064	4.8
4 model-2	=	=	eq. 13; 14	2.0	0.2	0.505	7.8	1.263	67.0	2.050	6.1
5 model-2	=	Rusanov eq. 20	eq. 13; 14	2.9	0.2	0.494	15.7	1.238	82.9	2.019	10.4
6 model-2	=	Rusanov eq. 20	eq. 13; 14	2.9	0.06	0.493	16.7	1.254	73.2	2.000	14.0
7 model-2	=	Rusanov eq. 20	eq. 13; 14	2.9	0.03	0.495	14.8	1.245	78.8	1.979	18.9
8 model-2	=	Rusanov eq. 20	eq. 13; 14	2.0	0.03	0.490	19.7	1.238	82.9	1.921	38.3
9 model-3	=	Rusanov eq. 20	Morris eq. 17 V_b=0.	2.9	0.2	0.458	71.2	1.103	67.3	1.586	51.6
10 model-3	=	Rusanov eq. 20	Morris eq. 17 $V_b = -\theta V_{free}$	2.9	0.2	0.460	67.6	1.14	89.2	1.70	95.4

This reduces the value of the divergence of the velocity field, as well as its spatial variations that are associated with dissipative effects of bulk viscosity. Besides the reduction of the Mach number, the addition of the Rusanov flux to the continuity equation is mandatory, since it stabilizes the algorithm that tends to be unstable at low Mach numbers due to the amplifying effect on the values of pressure given by eq. (18) (for low Mach number, inter-particle pressure grows). This is a "penalty term" in the equation of state, that penalizes variations of density in fact promoting the incompressibility condition of the simulated flow. As already observed above, a shortcoming of the Rusanov flux approach is that, analytically, the mass conservation constraint is no longer satisfied. Fig. 6 is the time-plot of the averaged values of the velocity divergence div ($\underline{\mathbf{v}}$), indicative of incompressibility of the fluid, relating to different simulations belonging to Model-2. Moreover, as it can be inferred from tab. 3, the performances of Model-2 seem to improve slightly further, if, besides lowering of the velocity divergence (lowering Mach number) and adding of the stabilizing Rusanov flux, the resolution is also increased by lowering the spacing of particles (dp). This is evident from the comparison between Simulations 7 and 8 as is inferred from tab. 3 and from fig. 3b.

The general performances of simulations belonging to Model-2 are, to a different degree, within the assumed experimental error, if a variable dispersion is considered (fig. 4). Otherwise, if a constant dispersion is assumed, only Simulation 8 is roughly within the experimental error, while the other approaches seem to be still too dispersive. Moreover, by a simple inspection of fig. 7, the best fit of the computed crest to the experimental data is achieved by Simulation 8. The model shows a lower diffusivity than models 0 and 1 due to the different viscous terms formulation used in the momentum equation. The formulation has a 0-th order consistency and conserves angular particle momentum as well, which is a desirable feature but which probably is not extremely important for the simulated test case. It automatically adds a bulk viscosity which is not present in reality as the flow is supposed to be uncompressible: it has however been possible to verify that the effects of bulk viscosity are weakened by reducing the unphysical compressibility of the fluid with the Rusanov flux correction to the continuity equation.

Model-3

This model, in light of the theoretical analysis of its features, introduces a lower bulk viscosity than Model-2, but it is only applicable when the motion is irrotational in the case of a non Newtonian fluid (proof provided in a next paper). In fig. 8 the trend of Irr (irrotational coefficient, already introduced in previous section) over time, regarding Simulation 9 belonging to Model-3, is displayed. Simulation 9 shows a marked irrotational feature of the fluid (high values of Irr) during the first phase of the transient and a more rotational motion in the second phase when the debris is flowing down the inclined plane. Simulations 9 and 10 appear to be more satisfactory than the simulations belonging to Model-2, at least by considering both the indexes discussed in the previous paragraphs (figs. 3c, 4) and the arrival time at each of the gauges (tab. 3).

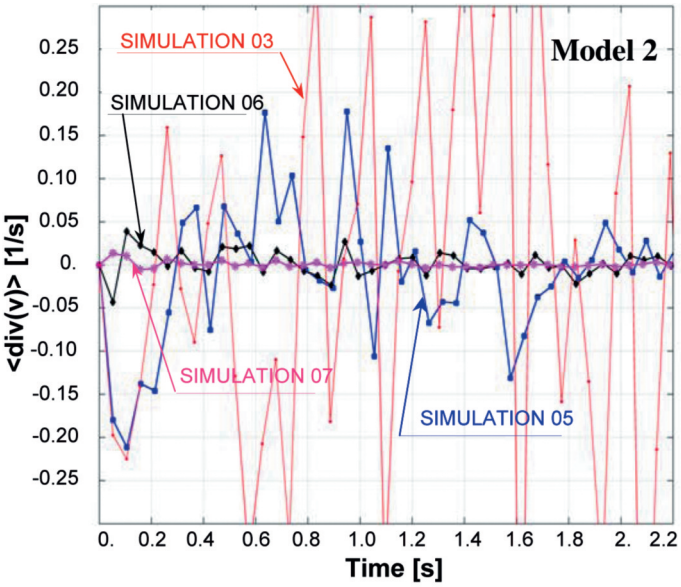

Fig. 6 - Numerical incompressibility trends of some simulations belonging to Model-2.

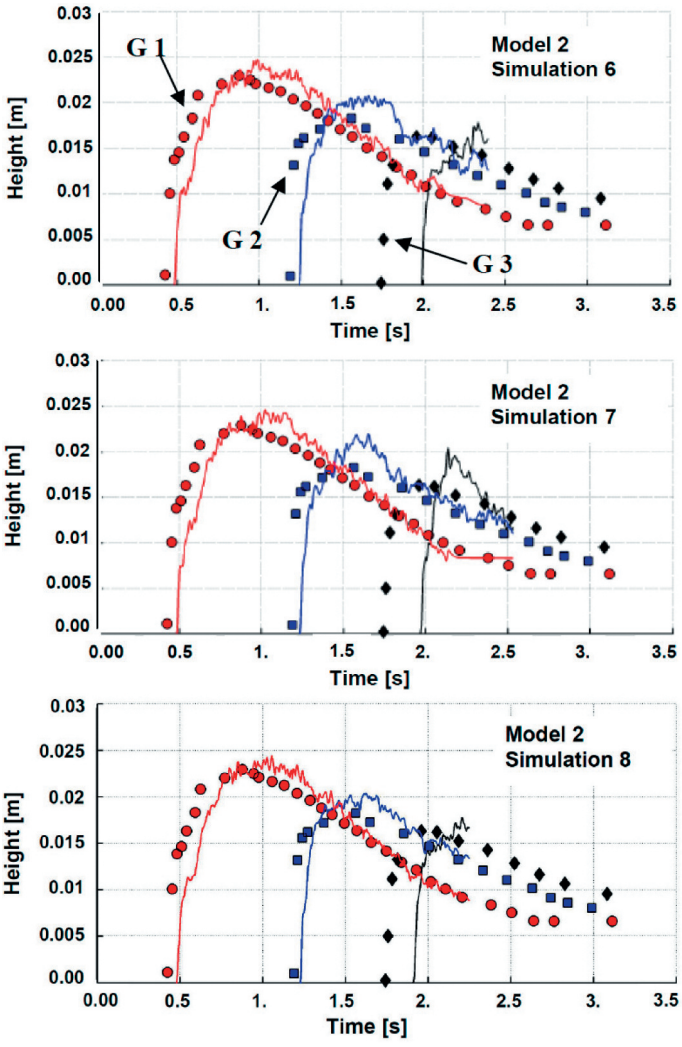

Fig. 7 - Comparison between the time plot of the simulated front heights obtained by Simulations 6, 7, 8 belonging to Model-2, and the corresponding experimental data (extrapolated from LAIGLE & COUSSOT, 1997) at three gauge locations.

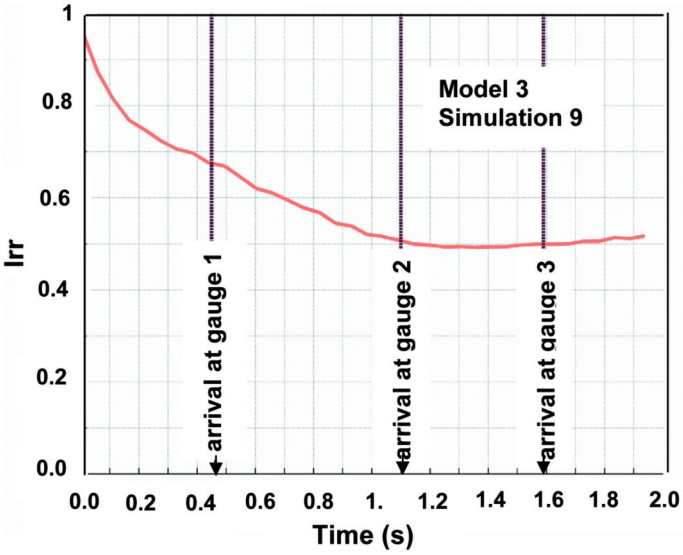

Fig. 8 - Trend of the flow regime obtained by Simulation 9 belonging to Model-3.

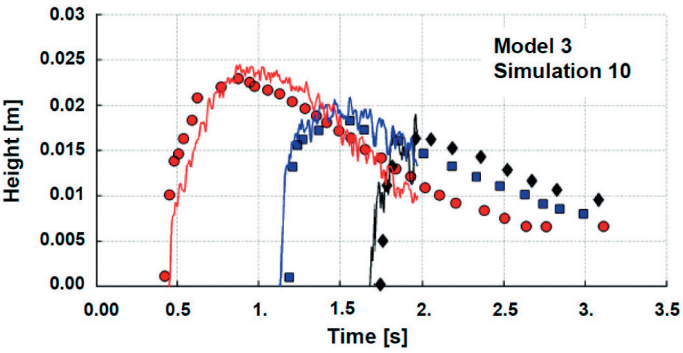

Fig. 9 - Comparison between the time plot of the simulated front heights obtained by Simulation 10 belonging to Model-3, and the corresponding experimental data (extrapolated from LAIGLE & COUSSOT, 1997) at the three gauges locations.

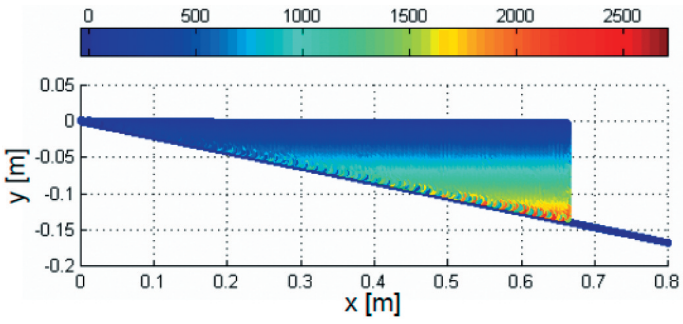

Fig. 10 - Initial particles disposition (lengths are in meters and particles are colour coded according to their pressure in Pa).

However, in theory, it should be applicable only during the first phase of the motion. It is worth noting that the arrival also of the front at the first gauge (in a flow range within which the Model-3 is theoretically applicable) is simulated in a better way than Model-2 even with relatively high Mach numbers and low resolution (tab. 3 and figs. 3c, 4). This suggests that Model-3 is less numerically diffusive than Model-2. Trends of Simulations 9 and 10 (tab. 3 and fig. 4) may also suggest that the Model-3 is slightly less viscous than the real phenomenon, since the numerical fronts anticipate the arrival time at the last two gauges, within the limits of experimental data accuracy, as previously discussed. Simulation 9 differs from Simulation 10 in a different way as to calculate the Morris wall particle velocity in the former case, a null velocity was assigned, while in the latter case a velocity opposite to the that of the free particles was assumed, as previously discussed (Morris $\underline{\mathbf{v}}_{\text{bound}} = -\theta \cdot \underline{\mathbf{v}}_{\text{free}}$). Fig. 9 shows that not only the arrival times, but also the crest profiles, provided by Simulation 10, fitted the data measured well. It is worth noting, from tab. 2 (comparing Simulations 8, 9 and 10) and from the discussion above, that an increase in the number of particles, does not necessarily result in an improvement of performances. When modeling problems characterized by advancing fronts, where it is important to estimate the viscous effects on the boundaries, which in turn influence the speed of the front itself, we found that the approach of Monaghan causes an excessive detachment of free particles (or 'real' as opposed to the definition of Ghost Particles) from the boundaries (due to excessive repulsion forces).

This detachment creates problems in estimating the viscous interactions. On the other hand, Morris particles allow free particles to maintain a distance from the boundaries close to the initial values throughout the entire simulation.

NUMERICAL DEBRIS FLOW PROFILE PLOTS

In this paragraph plots relating to calculated debris flow profiles are reported. For all the simulations performed, the first step was the computation of the initial hydrostatic pressure distribution. This target was achieved after a certain number of damped time steps, performed as in MONAGHAN (1994). Fig. 10 shows the initial particle disposition, common to all simulations, immediately before opening of the gate. The resulting pressure distribution, after the appropriate different number of time steps (tab. 2), is shown.

It is possible to see in the figure that a number of boundary effects are still present, causing small oscillations in pressure values close to the bottom of the flume. It was not however possible to completely remove them by increasing for example the number of time steps. It is however important to notice that the same plots with smoothed values for pressure would provide the exact hydrostatic distribution everywhere, regardless of boundaries. In fig. 11 velocity and pressure profiles, provided by Simulation 8 belonging to Model 2, at three different times after opening of the gate, are shown. It is interesting to note that pressure distributions are particularly reasonable according to particle position with respect to the free surface crests. We decided to show the Simulation 8, instead of Simulation 9 or 10, as the former was carried out with a higher resolution than that used for the latter simulations. In fig. 11d, concerning the first instants of the simulations it is possible to see an inner core in the fluid where the pressure values are still very close to the hydrostatic values highlighting the areas where the material has not moved yet. This is coherent with the velocity distribution plot of fig. 11a. In the subse-

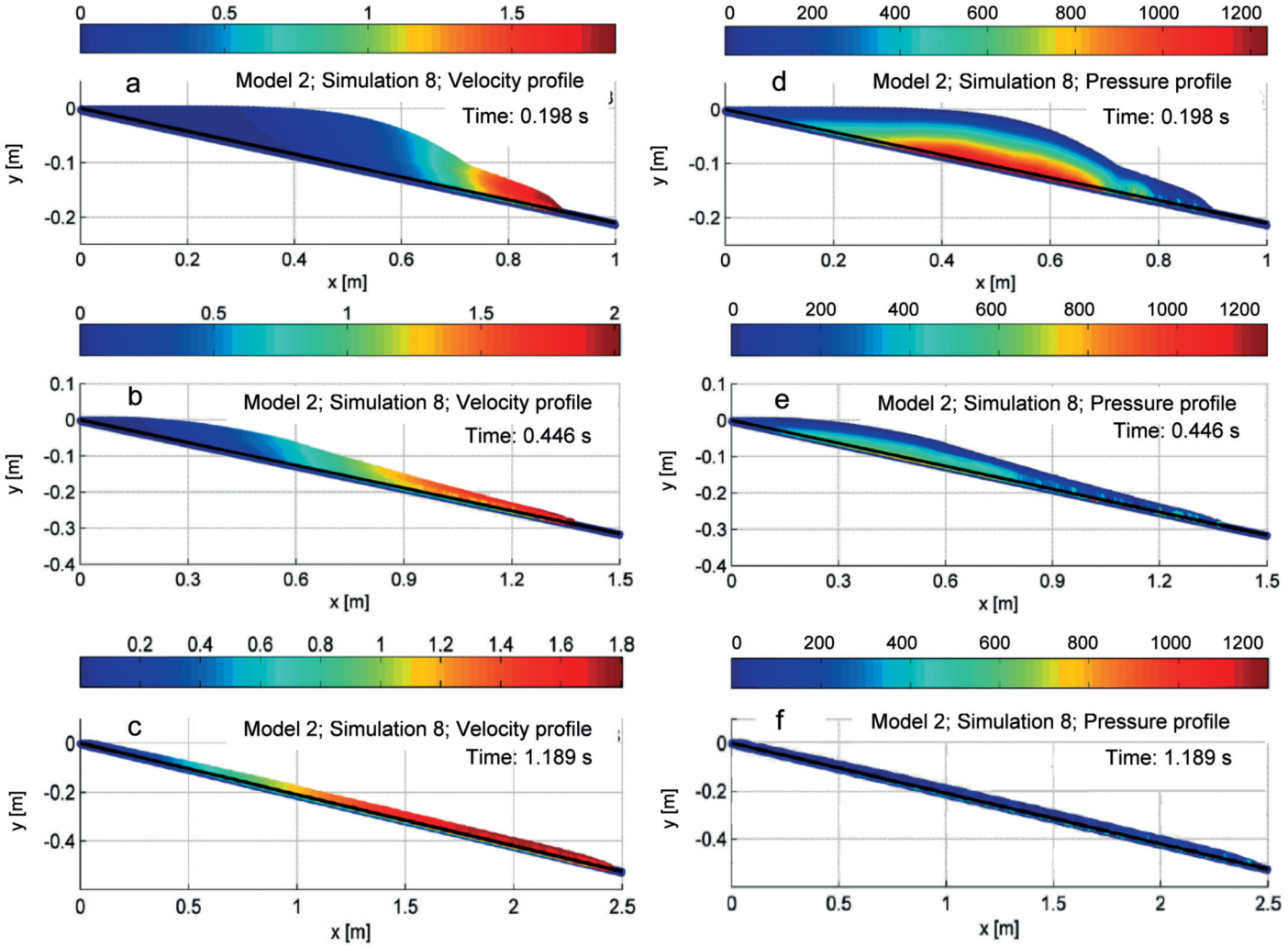

Fig. 11 - Velocity and pressure profiles of particles, Simulation 8 belonging to Model 2, at three different time after gate opening (particles are colour coded according to the module of their velocity in m/s at left, according to their pressure in Pa at right).

quent figures, all the material is moving (figs. 11b and 11c) and the pressure distribution seems to be more uniform. The higher uniformity of pressure distribution (figs. 11e and 11f) is also due to the reduced effect of weight caused by the front thinning. The corresponding profiles (not reported) related to Simulations 9 and 10, show structure of the pressure that is more complex, but consistent not only with the hydrostatic pressure, but also with the dynamic pressure. Further details will be provided in subsequent articles.

CONCLUSION

Different SPH approaches, incorporating the Herschel-Bulkley non Newtonian rheology, were developed to simulate a fast flow. In order to compare their performances, both reciprocally and with respect to the mudflow dam break experiment proposed by Laigle & Coussot (1997), numerical tests were performed. In particular, attention was focused on the calculated front arrival times at three successive gauges. Crest profile distributions have been discussed through plot inspections. Due to the inevitable difficulties in performing measurements on this kind of phenomena, even when carried out in laboratory, a reasonably adequate discussion of experimental errors has been developed. For these reasons, an index based on simple probabilistic considerations has been introduced in addition to direct comparison between the estimated experimental data and the numerical arrival times, with the purpose of assessing numerical performances of the simulations within a reasonable margin of experimental errors. The implemented SPH models, within a research code, are fully 2D and are therefore capable of providing more information than other more simplified approaches such as the 1D model, in particular as far as turbulence phenomena and rotational flows are concerned. The preliminary model discussed by the authors in previous papers (Minatti & Pasculli, 2011) provided numerically diffusive results, still being able to produce a good enough agreement with experimental results. Then three further different kinds of SPH models, proposed by different authors and, when necessary, adapted to be implemented for the test case discussed, were used. The implemented models employed different formulations for continuity and momentum equations, particle viscosity and boundary treatment. The first explored model, characterized in particular by the addition of the artificial vis-

cosity proposed by MONAGHAN & GINGOLD (1983), does not provide acceptable results, while the results obtained through the other two models seem to match, to a varying degree, the experimental data. Nevertheless, the best results were achieved by the addition of the Rusanov flux terms within the equation of continuity (preserving the usual approach for the momentum equation), providing a more accurate calculation of the weakly compressible flow (FERRARI *et alii*, 2009). This improved performance enhances, in particular, the computational accuracy of pressure through the equation of state. As reported by FERRARI *et alii* (2009), the introduction of such flux terms makes the model particularly suitable for simulating fast flow and dam break type problems without adding artificial viscosity terms in momentum equation, as performed by MONAGHAN (1994), but using only the terms due to pressure gradients and physical viscosity in the momentum equation. Another influencing feature, that further improves the results obtained through the Rusanov flux, regards the viscosity term of the momentum equation, proposed by MORRIS *et alii* (1997) and the value for the wall particle velocity proposed in the same article, aimed at correctly enforcing no slip conditions. Although the SPH approach shows certain drawbacks in simulating boundaries and so far no definitive and unique solution to the problem exists, its particular features for the reproduction of the free surface and for the simulations of very complex fluid-dynamics phenomena are encouraging for the further exploration of this type of approach in the field of debris flow.

ACKNOWLEDGMENTS

This work was supported by MIUR funds, under "PRIN 2010-2011" (Dept. of Engineering and Geology, Univ. of G. d'Annunzio Chieti-Pescara). The authors gratefully acknowledge the effort of two anonymous reviewers for their useful suggestions.

APPENDIX. NOTATION

The following symbols are used in this paper:

- B = constant parameter: 10 (s);
- c = artificial speed of sound ($m \cdot s^{-1}$);
- CFL = Courant-Friedrichs, Lewy's condition;
- d_f = normal distance of the selected free particle from the boundary (m);
- d_w = normal distance of the involved boundary (wall) particle (m);
- dp = initial fluid particles spacing (m);
- $\underline{\mathbf{f}}$ = body force per unit of mass (m) $(s)^{-2}$;
- g = acceleration due to gravity = 9.8 (m) $(s)^{-2}$;
- h = smoothing length (m);
- h_i = smoothing length of the *i*-th particle (m);
- h_{ij} = $(h_i + h_j)/2$; symmetrised smoothing length (m);
- H = maximum initial dam height (m);
- $\underline{\underline{\mathbf{I}}}$ = unit tensor = $\begin{pmatrix} 1 & 0 \\ 0 & 1 \end{pmatrix}$ (dimensionless);
- k = $g \cdot H$ $(m^2 \cdot s^{-2})$;
- K = liquid consistency $(Pa \cdot s^n)$;
- m_i = *i*-th particle mass (kg);
- M = Mach number (dimensionless);
- n = power law index (dimensionless);
- $N(\cdot)$ = normal probability density distribution;
- p = isotropic pressure (Pa);
- p_i = *i*-th particle pressure(Pa);
- $Pr(\cdot)$ = probability;
- $\underline{\mathbf{r}}_i$ = *i*-th particle position (m);
- $\underline{\mathbf{r}}_{ij}$ = distance between two interacting particle: $\underline{\mathbf{r}}_i - \underline{\mathbf{r}}_j$ (m);
- R = $(|\underline{\mathbf{x}} - \underline{\mathbf{x}}'|)/h$ ratio between particle distances and smoothing length (dimensionless);
- $\underline{v}_i$ = *i*-th component of the velocity vector $(m \cdot s^{-1})$;
- $\underline{\mathbf{v}}_{ij}$ = relative velocity between two interacting particles: $\underline{\mathbf{v}}_i - \underline{\mathbf{v}}_j$ $(m \cdot s^{-1})$;
- $\underline{\mathbf{v}}$ = velocity vector $(m \cdot s^{-1})$;
- $\underline{\mathbf{v}}_{bound}$ = boundary particle velocity vector $(m \cdot s^{-1})$;
- $\underline{\mathbf{v}}_{free}$ = free particle velocity vector $(m \cdot s^{-1})$;
- $W(\cdot)$ = kernel function;
- x_i = *i*-th particle positions in the given frame of reference (m);
- $\underline{x}$ = position vector of the selected particle (m);
- $\underline{x}'$ = position vector of a particle enclosed within the tributary area of the selected particle (m);
- $X_{at,k}$ = debris front arrival time at the k-th gauge (s);
- $X_{num,k}$ = calculated debris front arrival time at the k-th gauge (s);
- z_k = normalized statistical variable (dimensionless);
- α, β = coefficients related to artificial viscous term (dimensionless);
- δ = Dirac function;
- ΔA_j = tributary area associated with the particle j-th $(m)^2$;
- Δt = time step (s);
- $\underline{\underline{\boldsymbol{\varepsilon}}}$ = strain rate tensor (s^{-1});
- $\| \underline{\underline{\boldsymbol{\varepsilon}}} \|$ = strain tensor (square) Norm (s^{-1});
- η = dynamic shear viscosity (Pa·s);
- η_{ij} = symmetrised dynamic viscosity between interacting particles, such that $\eta_{ij} = \eta_{ji}$ (Pa·s);
- η_{max} = maximum viscosity value related to the regularization of the rheological law (Pa·s);
- η_p = local regularized dynamic viscosity of the fluid (Pa·s);
- λ = multiplicative statistical constant (dimensionles);
- μ_k = statistical mean equal to the value assessed from experiments (arrival time) (s);
- Π_{ij} = artificial viscous term (Pa·s);
- θ, θ_{max} = constant coefficients related to Morris boundary particles velocity (dimensionless);
- ρ = local density of the continuum $(kg \cdot m^{-3})$;
- ρ_0 = reference density of the fluid at zero pressure $(kg \cdot m^{-3})$;
- τ_c = yield stress (Pa);
- $\underline{\underline{\boldsymbol{\sigma}}}$ = total stress tensor (Pa);
- $\underline{\underline{\boldsymbol{\omega}}}$ = vorticity tensor $(s)^{-1}$;
- Ω_x = support domain $(m)^2$
- ξ = bulk viscosity coefficient (Pa·s);
- ψ = ratio between the boundary and the fluid particles spacing (dimensionless).

Mathematical symbols

- $|\underline{\mathbf{v}}|$ = modulus of the vector $\underline{\mathbf{v}}$;
- $\bullet$ = symbol of the scalar product;
- $\| (\cdot) \|$ = Norm of $(\cdot)$;
- $\frac{D}{Dt}(\cdot)$ = Material derivative of $(\cdot)$;
- ∇ = Nabla operator;
- $\nabla (\cdot)$ = Gradient of $(\cdot)$;
- $\nabla \bullet (\cdot)$ = Divergence of $(\cdot)$.

REFERENCES

ATKIN R.J. & CRAINE R.E. (1976) - *Continuum theories of mixtures: basic theory and historical development*. Q.J. Mech. Appl., **29** (2), 209-244.

BENZ W. (1988) - *Applications of Smooth Particle Hydrodynamics (SPH) to astrophysical problems*. Computer Physics Communications, **48** (1), 97-105.

CHAMBON G., BOUVAREL D., LAIGLE D. & NAAIM M. (2011) - *Numerical simulations of granular free-surface flows using smoothed particle hydrodynamics*. Journal of Non Newtonian fluid Mechanics, **166**, 698-712.

CHUNG T.J. (2006) - *Computational Fluid Dynamics*. Cambridge University Press, New York.

CLEARY P.W. (1998) - *Modelling confined multi-material heat and mass flows using SPH*. Appl. Math. Modelling, **22**, 981-993.

COUSSOT P. (1994) - *Steady, laminar, flow of concentrated mud suspensions in open channel*. Journal of Hydraulic Research, **32** (4), 535-559.

COUSSOT P. & MEUNIER M. (1996) - *Recognition, classification and mechanical description of debris flows*. Earth-Sci. Rev., **40**, 209-227.

COUSSOT P., LAIGLE D., ARATTANO M., DEGANUTTI A. & MARCHI L. (1998) - *Direct determination of rheological characteristics of debris flow*. Journal of Hydraulic Engineering, **124** (8), 865-868.

CROSTA G.B., CALVETTI F., IMPOSIMATO S., RODDEMAN D., FRATTINI P. & AGLIARDI F. (2001) - *Granular Flows and Numerical Modeling of Landslides. Debrisfall Assessment in Mountain Catchments for local end-users*. Contract N. EVG1-CT-1999-00007.

CRUDEN D.M. & VARNES D.J. (1996) - *Landslide types and processes*. Landslides Investigation and Mitigation: Transportation Research Board, US National Research Council, Special Report, **247**, Washington, DC., Turner A.K. & Schuster R.L. (ed.), 36-75.

ESPANOL P. & REVENGA M. (2003) - *Smoothed dissipative particle dynamics*. Physical Review, **67**, 026705.

FERRARI A., DUMBSER M., TORO E.F. & ARMANINI A. (2009) - *A new 3D parallel scheme for free surface flows*. Computers & Fluids, **38**, 1203-1217.

HUNGR O., EVANS S.G., BOVIS M.J. & HUTCHINSON J.N. (2001) - *A Review of the Classification of Landslides of the Flow Type*. Environmental & Engineering Geoscience, **7**, 221-238.

IDELSOHN S.R., OÑATE E., CALVO N. & DEL PIN F. (2003) - *The meshless finite element method*. Int. J. Numer. Meth. Engng., **58**, 893-912.

IVERSON R.M. (1997) - *The physics of debris flows*. Reviews of Geophysics, **35** (3), 245-296.

IVERSON R.M., LOGAN M., LAHUSEN R.G. & BERTI M. (2010) - *The perfect debris flow? Aggregated results from 28 large scale experiments*. Journal of Geophysical Research Reviews of Geophysics, **115**. doi: 10.1029/2009JF001514.

JAMES F. (2006) - *Statistical Methods in Experimental Physics*. 2nd Edition World Scientific.

JOP P., FORTERRE Y. & POULIQUEN O. (2006) - *A constitutive law for dense granular flows*. Nature, **41**, 727-730.

KAJTAR J.B. & MONAGHAN J.J. (2008) - *SPH simulations of swimming linked bodies*. Journal of Computational Physics, **227**, 8568-8587.

LAIGLE D. & COUSSOT P. (1997) - *Numerical modelling of mudflows*. Journal of Hydraulic Engineering, **123** (7), 617-623.

LAIGLE D., LACHAMP P. & NAAIM M. (2007) - *SPH-based numerical investigation of mudflow and other complex fluid flow interactions with structures*. Comput. Geosci., **11**, 297-306.

LIU G.R. & LIU M.B. (2003) - *Smoothed Particle Hydrodynamics a meshfree particle method*. World Scientific Publishing.

LIU M.B. & LIU G.R. (2006) - *Restoring particle consistency in smoothed particle hydrodynamics*. Applied Numerical Mathematics, **56**, 19-36.

LIU M.B. & LIU G.R. (2010) - *Smoothed Particle Hydrodynamics (SPH): an Overview and Recent Developments*. Arch Comput Methods Eng, **17**, 25-76. doi: 10.1007/s11831-010-9040-7.

MINATTI L. & PASCULLI A. (2010) - *Dam break Smoothed Particle Hydrodynamic modeling based on Riemann solvers*. Advances in Fluid Mechanics VIII, WIT Transactions on Engineering Sciences, WIT Press 2010, **69**, 145-156 (ISSN 1743-3533). doi: 10.2495/AFM100131.

MINATTI L. & PASCULLI A. (2011) - *SPH numerical approach in modelling 2D muddy debris flow*. 5th International Conference on Debris-Flow Hazards Mitigation Mechanics, Prediction and Assessment Padua 15-17 June 2011. doi: 10.4408/IJEGE.2011-03.B-052; Italian Journal of Engineering Geology and Environment-book Casa Editrice Università La Sapienza Roma ISBN 978-88-95814-46-9; ISSN 1825-6635.

MONAGHAN J.J. & GINGOLD R.A. (1983) - *Shock simulation by the particle method SPH*. Journal of Computational Physics, **52** (2), 374-389.

MONAGHAN J.J. (1994) - *Simulating free surface flows with SPH*. Journal of Computational Physics, **110**, 399-406.

MONAGHAN J.J. (2005) - *Smoothed particle hydrodynamics*. Reports on Progress in Physics, **68**, 1703-1759.

MONAGHAN J.J. & KAJTAR J.B. (2009) - *SPH particle boundary forces for arbitrary boundaries*. Computer Physics Communications, **180**, 1811-1820.

MORRIS J.P., FOX P.J. & ZHU Y. (1997) - *Modeling low Reynolds number incompressible flows using SPH*. Journal of Computational Physics, **136**, 214-226.

PAPANASTASIOU T.C. (1987) - *Flows of materials with yield*. Journal of Rheology, **31** (5), 385.

PÖSCHEL T. & SCHWAGER T. (2005) - *Computational Granular Dynamics*. Springer Berlin Heidelberg, New York.

RODRIGUEZ-PAZ M.X. & BONET J. (2003) - *A corrected Smooth Particle Hydrodynamics Method for the Simulation of Debris Flows*. Numerical Method of Partial Differential Equation, 140-162.

TAKAHASHI T. (2001) - *Mechanics and simulation of snow avalanches, pyroclastic flows and debris flows*. Special Publ. of the International Association of Sedimentologists. McCaffrey W.D., Kneller B.C., Peakall J., Editors by Blackwell Science, **31**, 11-43.

TAKEDA H., MIYAMA S.M. & SEKIYA M. (1994) - *Numerical simulation of viscous flow by smoothed particle hydrodynamics*. Progress of Theoretical Physics, **92**, 939-960.

TORO E.F. (2009) - *Riemann Solvers and Numerical Methods for Fluid Dynamics. A Practical Introduction*. Springer.

VARNES D.J. (1954) - *Landslide types and processes*. Landslides and Engineering Practice, Special Report, **28**, Highway Research Board, National Academy of Sciences, Washington, DC., Eckel E.B. Editor, 20-47.

VILA JP. (1999) - *On particle weighted methods and smooth particle hydrodynamics*. Math. Model Methods Appl. Sci., **9**, 161-209.

WENDLAND H. (1995) - *Piecewise polynomial, positive definite and compactly supported radial functions of minimal degree*. Advances in Computational Mathematics, **4**, 389-396.

Manuscript received 11 February 2012; accepted 4 January 2013; editorial responsability and handling by F. Guadagno.